Dalton Transactions

Investigation of the physical, optical, and chemical properties of phase segregated AlCoOx thin films from a novel hexol-type cluster

Journal:	*Dalton Transactions*
Manuscript ID	DT-ART-11-2020-003899.R1
Article Type:	Paper
Date Submitted by the Author:	20-Jan-2021
Complete List of Authors:	Levine, Jordan; University of Oregon, Department of Chemistry and Biochemistry Sharps, Meredith; University of Oregon, Department of Chemistry and Biochemistry Cochran, Elizabeth; University of Oregon, Department of Chemistry and Biochemistry; University of Oregon Marsh, David; University of Oregon, Department of Chemistry and Biochemistry Casey, William; University of California, Department of Chemistry Johnson, Darren; University of Oregon, Department of Chemistry and Biochemistry

ARTICLE

Investigation of the physical, optical, and chemical properties of phase segregated AlCoOx thin films from a novel hexol-type cluster

ALReceived 00th January 20xx,
Accepted 00th January 20xx

DOI: 10.1039/x0xx00000x

Jordan D. Levine,[a] Meredith C. Sharps,[a] Elizabeth A. Cochran,[a] David A Marsh,[a] William H. Casey,[b] Darren W. Johnson[a] *

The use of a novel inorganic nanoscale cluster ($Al[(u\text{-}OH)_2Co(NH_3)_4]_3(NO_3)_6$) was investigated for its utility as a precursor for AlCoOx films. Mixed-metal aluminum and cobalt oxide thin films were solution deposited from the novel cluster solution via the spin-coating method on Si (100) and quartz substrates. The films were annealed at increasing temperatures up to 800 °C, and characterization of these films via TEM and XRD confirms binary Co_3O_4 crystalline phase present in an amorphous Al_2O_3 network. Films are relatively smooth (R_{rms} < 4 nm), polycrystalline, and demonstrate a tunable optical response dominated by Co_3O_4 with two electronic transitions.

Introduction

Mixed-metal oxides are an extremely versatile material due to their attractive thermal, electronic, and optical properties, which has led to their extensive use in a variety of fields ranging from photovoltaics to thin film transistors.[1-3] The recent push towards more cost effective and less energy intensive processing of these materials has led to the utilization of solution-based deposition methods that allow for the potential of scalable and inexpensive fabrication of high quality metal oxide thin films.[4,5] While sol-gel techniques offer the benefits of solution-based fabrication, they often have the potential to leave behind organic contaminants which can be detrimental to film formation and/or properties.[6] Nanoscale inorganic clusters are a promising alternative precursor for solution processing of thin films because their precondensed metal-hydroxy network and nitrate counterions can more readily condense to form films with fewer morphological defects. Upon annealing of these films, nitrate counterions decompose and solvent evaporates, initiating the formation of a metal hydroxy species $M(OH)_x$. From here, further annealing can remove any remaining solvent and counterions, condensing the metal hydroxy network into the final metal oxide.

Nadarajah et. al. has shown the benefits of inorganic clusters, utilizing heterometallic gallium and zinc nanoscale clusters to form high quality IGZO thin film transistors that exhibit higher channel mobility than analagous metal nitrate and sol gel films.[7] Additional work by Jo et. al utilized the flat-Al_{13} cluster to produce aluminum oxide dielectrics with ultralow processing temperatures via a UV-light activation process, showing that the use of the cluster leads to more dense films than analogous metal nitrate films due to the cluster's high aluminum to nitrate ratio.[8] These advancements in the field have ultimately raised the profile of inorganic clusters as thin film precursors for a variety of applications in electronics and roll-to-roll processing.[9,10] While processing conditions are continually being optimized to realize more energy efficient thin film fabrication techniques, it is also vitally important to continue to investigate potential precursor compositions for solution deposition.

Inspired by the successful incorporation of clusters into films and devices, our lab previously reported a novel nanoscale cluster modelled after Werner's famous hexol (Fig 1, M=Co), notable as the first compound to exhibit molecular chirality without the presence of any carbon.[11,12] Due to their outer sphere nitrate counterions, preorganized structure, and low decomposition temperature, this class of clusters are a viable candidate to be investigated as precursors for solution deposited thin films.

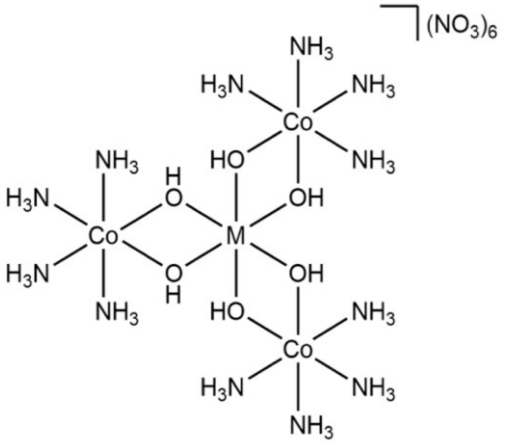

Fig. 1. Werner's famous hexol (M=Co). For this work, M=Al was used as the thin film precursor.

[a] Department of Chemistry & Biochemistry and Materials Science Institute, University of Oregon, Eugene, Oregon 97403-1253
[b] Department of Chemistry, University of California, Davis, California 95616.

† Footnotes relating to the title and/or authors should appear here.
Electronic Supplementary Information (ESI) available: [details of any supplementary information available should be included here]. See DOI: 10.1039/x0xx00000x

We previously reported the synthesis and characterization of a series of heterometallic hexol-type clusters (M[(μ-$OH)_2Co(NH_3)_4]_3(NO_3)_6$ M= Al, Ga, In).[11] As a proof of concept for the use of these hexol-type clusters as thin film precursors, the aluminum cobalt cluster ($Al[(u\text{-}OH)_2Co(NH_3)_4]_3(NO_3)_6$, **CoAl**) was investigated. This specific cluster was chosen because of its low decomposition temperature (Figure S1), as well as its heterometallic chemical composition which would allow for a direct comparison to similar films fabricated from Kast et. al.[4] In that work, the "flat" Al_{13} cluster was combined with $Co(NO_3)_2{\cdot}6H_2O$ at varying ratios in solution to produce a mixed metal oxide film that readily phase segregates into the corresponding oxides at 450 °C. This work highlighted the importance of studying heterometallic systems, and produced substantial precedent detailing the formation of mixed metal oxide films. In our current study we sought to investigate if the proposed **CoAl** cluster would produce similar results yielding the binary phase segregated oxides, or if the precondensed nature of the cluster would produce a homogenous distribution of cations throughout the film. Additionally, we sought to assess how temperature affects the morphological and microstructural properties of films made from a single source cobalt and aluminum precursor.

In this study, we demonstrate through microstructural, optical, and elemental characterization that the novel **CoAl** cluster is a suitable precursor for solution deposited thin films. We also confirm that despite the precondensed nature of the cluster, a phase segregated binary oxide is produced. To our knowledge, fabrication and characterization of these types of films have not been attempted, and these studies suggest that future work could lead to other derivatives of Werner's hexol being used for thin film fabrication.

2 Experimental

2.1 Preparation of precursor solution

Cobalt aluminum hexol-type clusters (**CoAl**) were fabricated using a previously reported procedure.[11] To synthesize the cluster, a 1.0 M aqueous solution of $Al(NO_3)_3{\cdot}9H_2O$ was added dropwise to a 0.5 M aqueous solution of $[Co(NH_3)_4(CO_3)](NO_3)$. The reaction was stirred at room temperature for 1 hour and was filtered and purified to yield the final **CoAl** cluster product. For the final precursor solution, a 0.4 M solution of the **CoAl** cluster was made in dimethyl sulfoxide (DMSO) and filtered through a 0.45 micron filter before deposition.

2.2 Film deposition and annealing

Single-side polished Si (100) was used for XRD, AFM, and XPS studies. Fused-quartz substrates were used for UV-Vis and XRR studies. All substrates were scored with a diamond scribe on the unpolished side and cleaved into 2 × 2 cm squares. Substrates were loaded into a Teflon boat that held the samples in a vertical orientation. Substrates were washed in a sonicator for 10 min in a solution of 6.25% Contrad 70, rinsed with nanopure (18.2 MΩ) water for 30 s, loaded onto a spin-coater, spin rinsed for 10 s, spin dried for 20 s at 2500 rpm, and placed on a hot plate at 100 °C for 2 min to finish drying. The substrates were then plasma cleaned in an O_2/N_2 mixture for 10 min, spin rinsed with nanopure water for 5 s, and spin dried for 25 s to remove any dust before the precursor solution was deposited.

Once substrates were prepared, the 0.4 M precursor solution was deposited dropwise from a syringe onto the substrate and spun for 150 s at 2500 RPM. The samples were immediately moved to a hot plate and annealed for 10 min at 250 °C. To fabricate multilayered films, as-spun samples were subjected to subsequent solution depositions and annealed at 250 °C on a hot plate until the desired number of layers was obtained. Samples were then post-annealed in a box furnace up to the desired temperature at a ramp rate of 12.5 °C/min and were annealed for 30 min at the allotted temperature.

2.3 Film Characterization

CoAl cluster bulk powder was analyzed using thermogravimetric analysis (TGA) on a TA instruments thermogravimetric analyzer, TGA Q500, by ramping from room temperature to 600 °C at a rate of 10 °C per minute under N_2 atmosphere. X-ray diffraction data was collected in a grazing incidence XRD (GIXRD) geometry on a Rigaku SmartLab with Cu Kα radiation (λ = 0.15418 nm). The incident angle of the X-ray beam was 0.5° relative to the sample plane, and the scintillation point detector was swept from 10° to 70° relative to the sample plane in 0.2° steps with an integration at each step of 30 s. Elemental composition was performed using a Thermo Scientific ESCALAB 250 X-XPS with an Al Kα monochromated source at 20 kV. Film thickness was determined through low-angle X-ray reflectivity (XRR) using a Bruker D8 Discover diffractometer, equipped with Cu Kα radiation and a Göbel mirror. Film thicknesses were determined by indexing the Kiessig fringes and using a modified version of Braggs law corrected for refraction. Atomic force microscopy (AFM) images were collected using a Bruker Dimension Icon atomic force microscope equipped with FastScan. Al-coated Si tapping mode probes were used, and images were collected over 1 μm^2 areas. Elemental composition and surface morphology images were determined by scanning electron micropscopy energy dispersive X-ray spectroscopy (SEM-EDS) using a ThermoFischer Helios Hydra Plasma FIB. Transmission electron microscopy (TEM) images were collected on an FEI Titan 80-300 equipped with a C_s image corrector with an accelerating voltage of 300KV. Samples were placed on a TEM grid using the focused ion beam on ThermoFischer Helios Hydra Plasma FIB. Transmittance measurements were collected on a PerkinElmer Lambda-1050 UV/vis/NIR spectrophotometer utilizing a 150 mm integrating sphere. Background samples were collected in air and with a blank quartz substrate. Transmittance data was collected from 300 nm to 800 nm at 1 nm intervals.

3 Results and discussion

The films' physical properties, morphology, and composition were studied through varying the number of deposited layers and annealing temperature. The spun-cast films were initially deposited from aqueous solutions even with significant varying of deposition parameters, films appeared to have undesirable surface defects and thus DMSO was utilized (Figure S2).

In order to investigate the crystal structure of the fabricated films, a GI-XRD annealing study was performed. Figure 2 shows the GI-XRD diffraction pattern of a **CoAl**-produced thin film annealed at 250 °C compared to films that were post-annealed at temperatures of 400 °C, 600 °C, and 800 °C. These diffraction patterns are referenced to

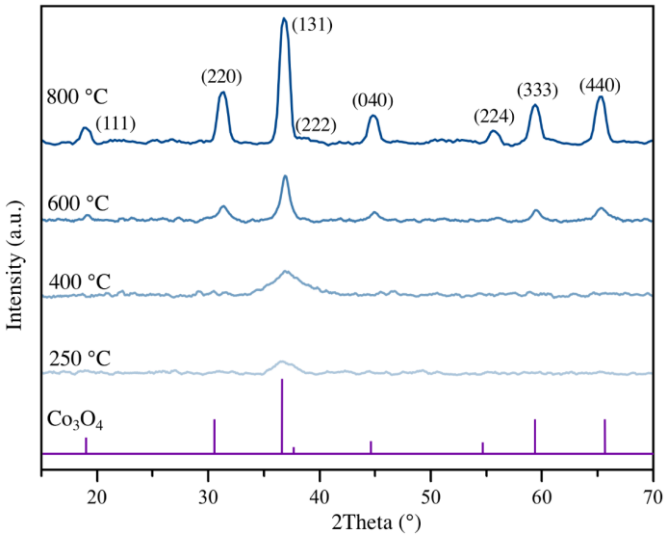

Fig. 2. GI-XRD diffraction patterns of **CoAl** films annealed at 250 °C, 400 °C, 600 °C, and 800 °C, referenced to Co_3O_4.

the Co_3O_4 diffraction pattern. The diffraction peaks at 2θ = 19.0°, 31.3°, 37.0°, 44.9°, 55.6°, 59.5°, and 65.4° can be indexed to (111), (220), (131), (040), (224), and (440) reflections in Co_3O_4 spinel, respectively. The initial hot plate anneal of films at 250 °C and films annealed at 400 °C exhibit the emergence of a crystalline phase in a mostly amorphous film network. By 800 °C, the crystallinity greatly increases and the diffraction pattern can be indexed to the Co_3O_4 spinel. [13] No other diffraction peaks were detected, suggesting that the cobalt present from the cluster crystallizes into the Co_3O_4 spinel crystal structure. However, due to the similarity in ionic radii of Co^{3+} and Al^{3+} , it can be difficult to exclude the possibility of Al^{3+} ions migrating into the Co_3O_4 spinel to form $CoAl_2O_4$ or Al Co_2O_4 spinel. While the cobalt oxide spinel and cobalt aluminate spinels have extremely similar diffraction patterns, there is a distinctive characteristic cobalt aluminate spinel peak at 2θ = 49.0° that is not present in our reported diffraction pattern.[14] After indexing the diffraction peaks present in the sample annealed at 800°C, Bragg's law was utilized to determine interplanar spacing and calculate lattice parameters.[15] The lattice parameter calculated from the diffraction pattern was determined to be *a* = 8.073(8) Å, closely matching that of Co_3O_4 (*a* = 8.072(3) Å) and somewhat lower than that of $CoAl_2O_4$ or $AlCo_2O_4$, where *a* = 8.106(6) Å and 8.087(2) Å, respectively. These initial results suggest that the cobalt present in the films crystallizes and phase segregates into a binary oxide containing crystalline Co_3O_4 present in an amorphous Al_2O_3 network.

To further understand the chemical composition of these films, XPS studies were performed. Figure 3 shows the cobalt 2p, aluminum 2p, and sulfur 2p XPS spectra of **CoAl** films that were annealed at 400 °C, 600 °C, and 800 °C. For cobalt, the peaks at 779.8 eV and 795.8 correlate to Co $2p_{3/2}$ and $Co_{1/2}$ respectively.[16] The satellite peaks indicate the presence of Co^{2+} and Co^{3+} oxiditation states which can be attributed to the presence of the Co_3O_4 spinel. Lastly, the modified Auger parameter (1553.1 eV), is consistent with previously reported Co_3O_4 films further suggesting the cobalt in these films is composed of Co_3O_4.[17] Additional analysis of the aluminum spectra supports the presence of Al_2O_3. The peak at 74.1 eV correlates to the aluminum 2p line and is in agreement with previously reported Al_2O_3 thin films.[18] Lastly, we investigated the sulfur content of these films. The films annealed at 400 °C and 600 °C show small amounts of sulfur (~1.0 at. %) from residual DMSO present as sulfate in the films. However, further annealing to 800 °C appears to remove all residual sulfur from the film.

With a clearer understanding of the composition of these films, we sought to further investigate their physical and morphological

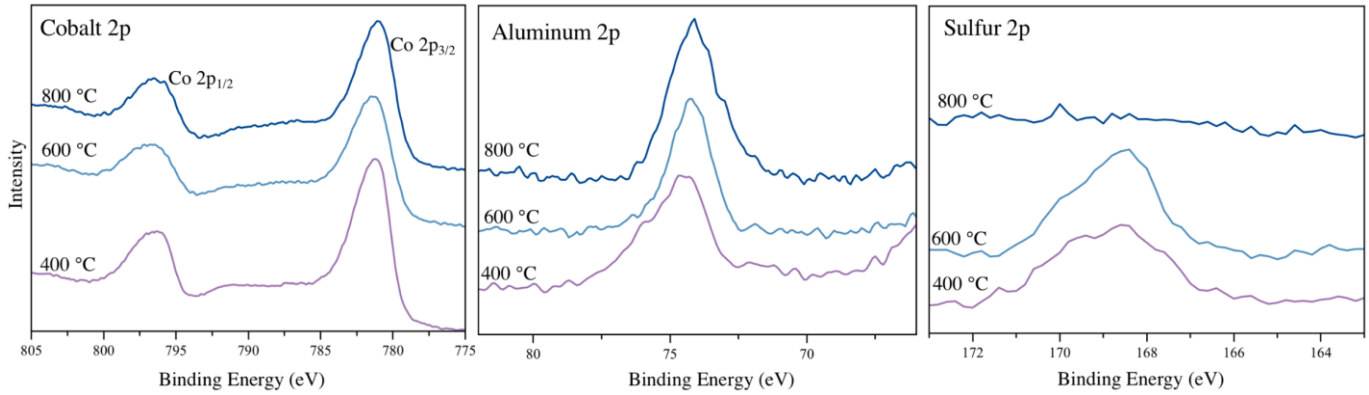

Fig. 3. Cobalt 2p (left), aluminum 2p (middle), and sulfur 2p (right) XPS spectra of 1-layer **CoAl** films annealed at 400 °C, 600 °C, and 800 °C.

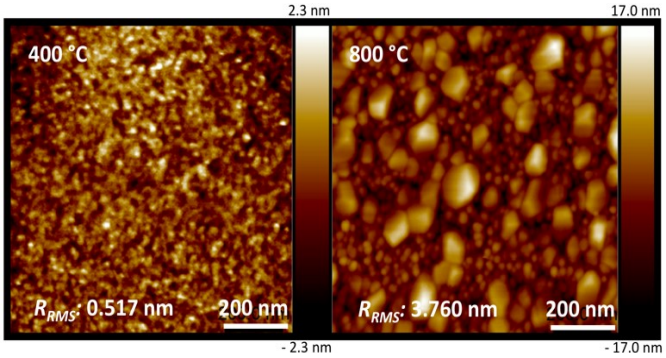

Fig. 4. 1 μm² area AFM scans of 5-layer **CoAl** films annealed at 400 °C (left) and 800 °C (right).

properties. XRR analysis determined single layer films films to be roughly 22.0 nm thick with each additional layer increasing the thickness by approximately 20.5 nm (Figure S3). XRR analysis determined single layer films to be roughly 22.0 nm thick with each additional layer increasing the thickness by approximately 20.5 nm (Figure S3). Figure 4 shows the AFM scan of 5-layer **CoAl** films annealed at 400 °C and 800 °C. At 400 °C, the films approach near-atomic roughness with an R_{rms} of 0.517 nm. By increasing the annealing temperature to 800 °C, the roughness of the films is increased roughly 7-fold to an R_{rms} = 3.760 nm due to the apparent emergence of crystallites on the surface.

A scanning electron miscroppy (SEM) investigation of these films shows the emergence and growth of crystallites as annealing temperature is increased (Figure 5). Additionally, SEM-EDS analysis was carried out to further probe elemental distribution and (approximate) ratio of the cobalt and aluminum in the film. Results in Figure 5 indicate a uniform distribution of aluminum and cobalt throughout the film at each annealing temperature. This suggests that the Co_3O_4 crystallites propagate throughout the film, supported by an amorphous alumina matrix , and are not just present at the surface. EDS analysis also confirmed a final film composition of 3 parts cobalt to 1 part aluminum, matching that of the starting **CoAl** cluster. This was expected due to the non-volatility of the deposited ions and previous work demonstrating the trend between precursor and final film composition in solution-processed spin-cast films. [7,19]

To further probe the phase segregation apparent in these films, TEM images were collected. Figure 6 shows high-resolution TEM cross section prepared by focused ion milling of a 1-layer **CoAl** film

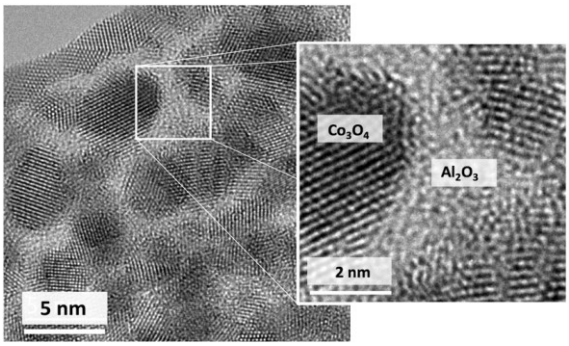

Fig. 6. TEM image of 1-layer CoAl film annealed at 800 °C showing clear crystalline and amorphous domains.

annealed at 800° C. The milling occurred in a region of the film that did not contain any of the larger crystallites present at the surface. Analysis of TEM images and electron diffraction pattern (Figure S4) further confirmed a polycrystalline film with a crystal structure matching the *d*-spacing of Co_3O_4. The TEM image also shows that the Co_3O_4 crystallites propogate throughout the entire film, supported by an amorphous Al_2O_3 matrix.

Analysis of SEM and TEM images suggest a variation in crystallite size as a function of annealing temperature. To further evaluate the size of crystalline domains in each film, the Scherrer equation was utilized :

$$d = \frac{K \cdot \lambda}{\beta \cdot cos\theta} \qquad (1)$$

where d is the crystallite size, K is the Scherrer constant, λ is X-ray wavelength, β is the peak width (FWHM), and θ is the corresponding Bragg angle.[20] Table 1 displays the average crystallite size of the Co_3O_4 domains, displaying a near linear correlation between crystallite size and annealing temperature.

With a full understanding of the composition in these **CoAl** films, we sought to investigate the optical properties of the fabricated films. Upon annealing, the deposited films appeared pale brown and transparent.The absorbance properties of the hot plate annealed and box furnace post-annealed layered films were studied between 300 and 800 nm. Upon the post-annealing of the films, the absorbance of the films decreases as shown in Figure S5. Figure 7a

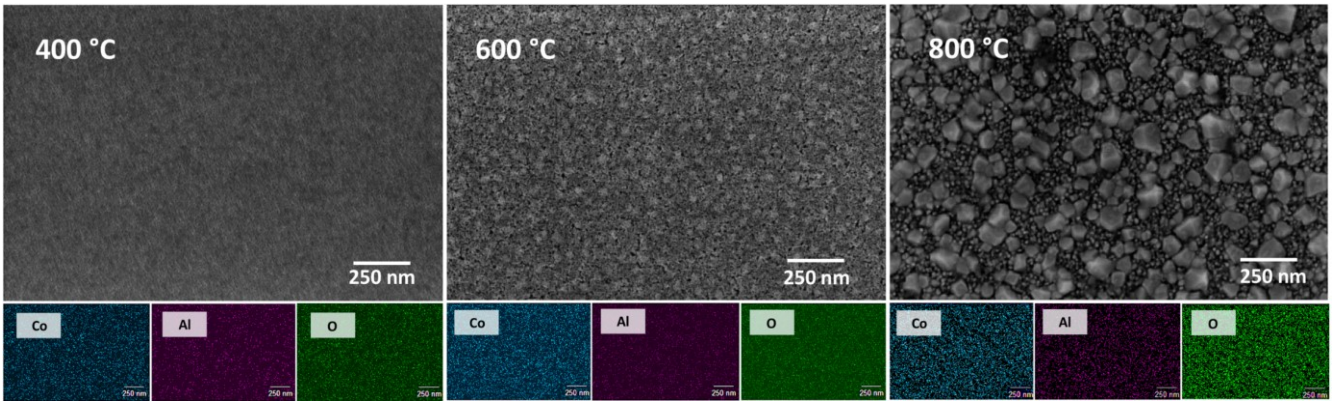

Fig. 5. (Top) SEM images of **CoAl** films annealed at 400 °C, 600 °C, and 800°C with corresponding EDS scans of cobalt, aluminum, and oxygen (bottom).

Table 1. Average crystallite size in **CoAl** films.

Annealing temp (°C)	Crystallite size (nm)
800	19.3
700	14.1
600	9.9
500	4.0

shows the absorbance spectra for the post-annealed **CoAl** films featuring 1-5 layers. A clear trend between the number of deposited layers and an increased absorbance can be discerned with a linear correlation between number of deposited layers and film absorbance at the λ_{max}. The two regions of optical transitions in the spectra correspond to the Co^{3+} 3d - Co^{2+} 3d at 685 nm and the O 2p – Co^{3+} 3d at 408 nm, consistent with previously reported Co_3O_4 films.[21,22] The optical response in these films is dominated by Co_3O_4, indicating that the amorphous alumina network does not contribute to the absorbance of these films in a significant manner. The observed optical data was further utilized to estimate the band gap energy for these films using the classical relation for optically induced transitions in semiconductors shown in equation 2:

$$\alpha = \frac{A(hv - E_g)^n}{hv} \qquad (2)$$

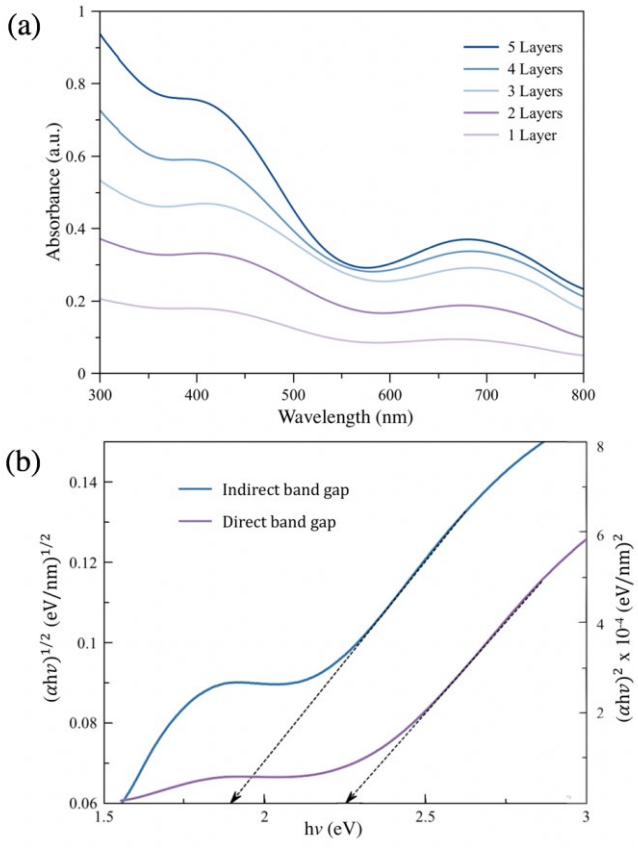

Fig. 7. (a) UV-vis spectra of 1-5 layer **CoAl** films annealed at 700°C. (b) Band gap analyses of direct and indirect optical transitions for 5-layer **CoAl** film annealed at 700 °C

where α is the absorption coefficient, A is a constant, hv is the photon energy, E_g is optical band gap, and n is ½ for direct transitions and 2 for indirect transitions.[23] Figure 7b shows the plots of $(\alpha hv)^2$ and $(\alpha hv)^{1/2}$ vs *hv* for the 5 layer **CoAl** film annealed at 700 °C. Since the linear extrapolation of each plot appears in the domain of higher as well as lower energies, it indicates the presence of both direct and indirect optical transitions in these films.[24] Extrapolation of the linear region of each plot to the axis gives the indirect and direct optical band gap energies of 1.89 eV and 2.25 eV, respectively. These results are slightly higher than previously reported spray pyrolysis Co_3O_4 films with the minor difference being attributed to the amorphous alumina network present in our **CoAl** films.[25]

The results presented show a clear picture for the composition and characterization of the fabricated films. Despite the precondensed nature of the **CoAl** cluster, films annealed at 400°C appear to phase segregate instead of forming an alloy. This can likely be attributed to cobalt's nonzero ligand field stabilization energy and low oxidation state indicating that the formation of an amporphous structure would be energetically unfavorable compared to a crystalline one.[4] When these films are annealed to 800 °C, the phase segregation becomes more apparent, with TEM analysis showing a binary oxide containing crystalline Co_3O_4 present in an amorphous Al_2O_3 network. This correlates with previous reports showing that cations with greater crystal field stabilization energy such as Co^{3+} will readily phase segregate into the corresponding oxide rather than form an amorphous aluminum oxide alloy.[26] We also present data investigating the crystallinity of these films. Annealed films are polycrystalline and the Co_3O_4 crystallite size grows almost linearly with temperature. This could perhaps be valuable for potential mixed metal oxide sytems studying capacitance where polycrystalline films are preffered to amorphous ones as long as crytallite size doesn't exceed film thickness.[27]

4. Conclusions

In this work, polycrystalline mixed-metal cobalt aluminum oxide films were fabricated from a novel hexol-type cluster. Films were solution deposited via spin-coating and post-annealed at varying temperatures up to 800 °C. By varying the number of layers deposited and annealing temperature, we were able to discern morphological, compositional, microstructural, and optical properties of these films. After spin coating and annealing the films up to 800 °C, the aluminum and cobalt phase segregate to form polycrystalline Co_3O_4 in an amorphous Al_2O_3 network. As annealing temperature increases, the Co_3O_4 crystallite size increases as well. The optical properties of these films can be tuned by varying the number of layers deposited, and the Co_3O_4 present in these films dominates the optical response, exhibiting both indirect and direct optical transitions. These results confirm that the **CoAl** cluster (Al[(u-$OH)_2Co(NH_3)_4]_3(NO_3)_6$) can be used as a precursor to produce high quality mixed metal oxide thin films. The successful fabrication and subsequent characterization of these films warrants future studies into similar films fabricated from hexol-type derivatives previously reported in literature.

Conflicts of interest

There are no conflicts to declare

Acknowledgments

This material was based on work in the Center for Sustainable Materials Chemistry, which was supported by the U.S. National Science Foundation under Grant CHE-1606982. This work was also supported by the Bradshaw and Holzapfel Research Professorship in Transformational Science and Mathematics to DWJ and the University of Oregon. MCS was supported by the NSF Graduate Research Fellowship Program under Grant No. 1309047. The authors acknowledge funding for shared instrumentation in the UO CAMCOR facilities, in addition to instrumentation support from Valerie Brogden and Joshua Raznik. We also acknowledge Catherine Page for her insight into this project.

References

1 P. L. Qin, H. W. Lei, X. L. Zheng, Q. Liu, H. Tao, G. Yang, W. J. Ke, L. B. Xiong, M. C. Qin, and X. Z. Zhao, *Adv. Mater.* Interfaces, 2016, **3**, 1500799.

2 A. Nadarajah, M. E. Carnes, M. G. Kast, D. W. Johnson, and S. W. Boettcher, *Chem. Mater.*, 2013, **25**, 4080−4087.

3 J. W. Hennek, M. G. Kim, M. G. Kanatzidis, A. Facchetti, and T. J. Marks., *J. Am. Chem. Soc.*, 2012, **134**, 9593–96.

4 M. Kast, E. A. Cochran, L. Enman, G.Mitchson, J.Ditto, C. Siefe and P. Plassmeyer, J. *Am. Chem. Soc.*, 2016, **138**, 16800–808.

5 E.A. Cochran, K.Woods, D.W. Johnson, C.J. Page, and S.W. Boettcher, *J. Mat. Chem.*, 2019, **42**, 24124–49.

6 C. J. Brinker and G. W. Scherer Academic Press, Inc., Boston, 1st edn, 1990.

7 A. Nadarajah, M. Z. B. Wu, K. Archila, M. G. Kast, A. M. Smith, T. H. Chiang, D. A. Keszler, J. F. Wager, and S. W. Boettcher, *Chem. Mater.*, 2015, **27**, 5587–96.

8 J. Jo, Y. Kim, J. Park, J. S. Heo, S. Hwang, W. Lee, M. Yoon, M. Kim, and S. K. Park. *ACS. APPL. MATER. INTER.,* 2017, **40**, 35114–24.

9 W. Xu, H. Li, J. Bin Xu and L. Wang, *ACS Appl. Mater. Interfaces*, 2018, **10**, 25878–25901.

10 A. Liu, H. Zhu, H. Sun, Y. Xu and Y. Noh, *Adv. Mater.*, 2018, **30**, 1706364.

11 D. A. Marsh, W.S. Elliott, R. M. Smith, M. C. Sharps, M. K. Baumeister, M. E. Carnes, L. N. Zakharov, W. H. Casey, and D. W. Johnson, *Angew. Chem. Int. Ed.,* 2017, **56**, 8776–8779.

12 A.Werner, *Ber.Dtsch. Chem. Ges.*, 1907, **40**, 2103 –2125.

13 J.P. Picard, G. Baud, J.P. Besse, and R. Chevalier, J. Less. *Common Met.*, 1980, **75**, 99-104.

14 H. S C. O'Neill, *Eur. J. Min.*, 1994, **6**, 603-609

15 J. Kacher, C. Landon, B. L. Adams and D. Fullwood, *Ultramicroscopy*, 2009, **109**, 1148–1156.

16 M. Oku and K. Hirokawa, *J. Electron Spectrosc.*, 1976, **8**, 475–481.

17 B. S. M. Kretzschmar, K. Assim, A. Preuß, A. Heft, M. Korb, M. Pügner, T. Lampke, B. Grünler and H. Lang, *RSC. Adv.,* 2018, **8**, 15632–15640.

18 C. S. Yang, J. S. Kim, J. W. Choi, M. H. Kwon, Y. J. Kim, J. G. Choi and G. T. Kim, *J. Ind. Eng. Chem.*, 2000, **6**, 149-156.

19 K.M. Norelli, P.N. Plassmeyer, K.N. Woods, B.A. Glassy, C. C. Knutson, M. Beekman, and C. J. Page. *Solid State Sci.*, 2016, **55**, 8− 12.

20 A. L. Patterson, *Phys. Rev.,* 1939, **56**, 978–982.

21 C. Cheng, M. Serizawa and H. Sakata, *Mater. Chem. Phys.*, 1998, **53**, 225-230.

22 P. S. Patil, L. D. Kadam, and C. D. Lokhande, *Thin Solid Films*, 1996, **272**, 29-32.

23 R.H. Misho and W.A. Murad, *Sol. Energ. Mat. Sol. C.*, 1992, **27**, 335.

24 V. R. Shinde, S. B. Mahadik, T. P. Gujar and C. D. Lokhande, *Appl. Surf. Sci.*, 2006, **20**, 7487–92.

25 L.D. Kadam, and P.S. Patil, *Mater. Chem. Phys.*, 2001, **68**, 225.

26 L.J. Enman, M. G. Kast, E. A. Cochran, E. Pledger, M. B. Stevens, and S. W. Boettcher, *J. Phys. Chem. C* , 2018, **25**, 13691–704.

27 D. M. Hausmann and R. G. Gordon, *J. Cryst. Growth*, 2003, **249**, 251–261.